Available online at www.sciencedirect.com
SCIENCE DIRECT®
International Journal of Heat and Mass Transfer 47 (2004) 729–742
International Journal of HEAT and MASS TRANSFER
www.elsevier.com/locate/ijhmt

Pool boiling heat transfer to electrolyte solutions

M. Jamialahmadi [a], A. Helalizadeh [b], H. Müller-Steinhagen [c,d,*]

[a] The University of Petroleum Industry, Ahwaz, Iran
[b] Department of Chemical and Process Engineering, University of Surrey, Guildford, UK
[c] Institute for Thermodynamics and Thermal Engineering, University of Stuttgart, Pfaffenwaldring 38-40, Stuttgart 70569, Germany
[d] Institute for Technical Thermodynamics, German Aerospace Research Centre (DLR), Germany

Received 5 December 2002; received in revised form 14 July 2003

Abstract

Pool boiling heat transfer coefficients were measured for solutions of salts with positive solubility in water. The effect of the dissolved salts on nucleation site density, bubble departure diameter and bubble frequency was also investigated. The results show that at low heat fluxes heat transfer coefficients can be considerably lower than corresponding values for distilled water. At high heat fluxes the negative effect of the dissolved electrolyte gradually decreased and finally some improvement in heat transfer coefficient was observed. A correlation was developed for nucleate boiling of aqueous solutions from salts with positive solubility. Assuming that the mass transfer resistance is limited to the liquid side, the proposed model allows the prediction of heat transfer coefficients from boiling point data of the respective solutions. Comparison with a significant number of experimental data for different systems indicates that the model should be sufficiently accurate for most practical applications.
© 2003 Elsevier Ltd. All rights reserved.

Keywords: Pool boiling; Salt solutions; Heat transfer; Mass transfer; Modelling; Correlation

1. Introduction

Pool boiling is a process of great practical significance. It has hence been the subject of intensive research for the past decades, covering both fundamental and applied aspects. Most of these research efforts have been expended on the boiling characteristics of pure liquids, while boiling of mixtures and solutions has less frequently been investigated. Experimental investigations on pool boiling of mixtures have shown, however, that the physical processes associated with multi-component boiling are significantly different from those for pure liquids.

Boiling of mixtures of organic liquids or of inorganic salt solutions is distinct from boiling of pure liquids in that the driving force for heat transfer is in turn governed by mass transfer. Therefore, the evaporation rate can be severely reduced for the mixtures because the rate of mass diffusion in the liquid phase is usually much slower than that of heat diffusion [1]. Van Wijk et al. [2] presented the physical explanation for the observed reduction of the mixture boiling heat transfer coefficient. They suggested that preferential evaporation of the more volatile component takes places at the heated surface such that the local boiling point rises. Sternling and Tichacek [3] provided three possible explanations:

1. The change in the mixture physical properties, notably viscosity with composition.
2. The change in the rate of bubble growth caused by the resistance to the mass transfer of the more volatile component in diffusing into the growing bubble, and
3. Changes in the rate of nucleation of new boiling sites on the surface.

According to the work of Thome [4,5] the decrease in the boiling heat transfer coefficient is a combined result

* Corresponding author. Address: Institute for Thermodynamics and Thermal Engineering, University of Stuttgart, Pfaffenwaldring 38-40, Stuttgart 70569, Germany. Tel.: +49-711-6862-358; fax: +49-711-6862-712.
E-mail address: hans.mueller-steinhagen@dlr.de (H. Müller-Steinhagen).

0017-9310/$ - see front matter © 2003 Elsevier Ltd. All rights reserved.
doi:10.1016/j.ijheatmasstransfer.2003.07.025

Nomenclature

a_0, a_1, a_2	constant in Eq. (4)
b_0, b_1	constant in Eq. (37)
B_0	the ratio of heat transfer surface to interfacial mass transfer area
C	concentration, kg/m^3
c_p	specific heat, kJ/kg K
D	mass diffusivity, m^2/s
d_b	bubble departure diameter, m
Δh_v	latent heat of evaporation, kJ/kg
I	ionic strength mol/m^3
j	mass flux by molecular diffusion, kg/m^2 s
m	molarity of ions, mole/m^3
n	mass flux, kg/m^2 s
p	pressure, bar
p_c	critical pressure, bar
p^*	saturation pressure, bar
p_r	reduced pressure, p^*/p_c
q	heat flux, W/m^2
r	defined by Eq. (20)
r_c	cavity radius, m
s	distance between thermocouple location and heat transfer surface, m
T	temperature, K
u	velocity with respect to a fixed coordinate, m/s
u_b	bubble rise velocity, m/s
U	mass average velocity, m/s
x	mass fraction
z	distance coordinate, m
Z	valence of the ions

Greek symbols

α	heat transfer coefficient, W/m^2 K
β	mass transfer coefficient, m/s
θ	defined by Eq. (23)
λ	thermal conductivity, W/mK
μ	dynamic viscosity, kg/m s
ρ	density, kg/m^3
σ	surface tension, N/m

Subscripts and superscripts

av	average
b	bulk or boiling
i	interface
id	ideal
0	reference condition
s	surface or solute
th	thermocouple
v	vapor
w	wall or water

of mixture effects on bubble growth rate, bubble departure diameter and boiling site density, and non-linear variation of the pertinent physical properties.

In comparison to pool boiling of organic liquid mixtures, far less information is available about the effect of dissolved salts on the mechanisms of boiling. Experimental data for heat fluxes below 50 kW/m^2 were reported in 1930 [6,7]. The reported heat transfer coefficients are extremely high. Knowles [8] studied subcooled boiling of river water on an electrically heated stainless steel tube that was centrally located in a glass tube, but his experiments were plagued by deposition of scale on the heating element. Tolubinsky and Ostrovsky [9] investigated sodium chloride solutions. Since their results did not differ from results measured in pure water, they concluded that the mechanism of bubble growth in aqueous solutions was affected only by the properties of pure water. Such a conclusion does not seem justified after taking into consideration results of Steinbrecht [10] and observations by Fritz [11] and Ceumern-Lindenstjerna [12]. Feldkamp [13] investigated pool boiling heat transfer of saccharose, sodium chloride and sodium hydroxide solutions for heat fluxes below 100 kW/m^2. The reported heat transfer coefficients are lower than those of distilled water but no bubble breakup was observed in this range of heat fluxes.

Boiling heat transfer of aqueous salt solutions is an essential operation in the manufacturing of almost all inorganic salts. Heat transfer occurs mostly in large heat exchangers or multiple-effect evaporators, which are often a major cost component of the total plant cost. Seawater with high ionic strength is also used in desalination plants to produce fresh water. The reliable prediction of heat transfer coefficients is therefore of major importance for optimum and economical overall plant design. Boiling characteristics of aqueous electrolyte solutions are likely to be different from those of organic mixtures because of the differences in surface tension, wetting characteristics and bubble coalescence and breakup behavior. Fundamental studies related to vapor bubble dynamic in pool boiling of electrolyte solutions highlight these differences [14].

The ultimate objective of any fundamental approach to this problem is to be able to predict the heat transfer coefficient for a given condition through the knowledge and understanding of the processes involved. In this investigation, systematic measurements of heat transfer coefficient and bubble size distribution were carried out over a wide range of heat fluxes and electrolyte concentrations. A unified model for the prediction of pool boiling heat transfer coefficients for electrolyte solutions is presented to correlate the available experimental data.

2. Experimental equipments and procedure

The complete pool boiling apparatus is shown in Fig. 1. The apparatus consists of a thick-walled cylindrical stainless steel tank containing 30 liters of test liquid and a vertical condenser to condense and recycle the evaporated liquid. The test section is mounted horizontally within the tank and can be observed and photographed through observation glasses at both ends of the tank. Tank and condenser are heavily insulated to reduce heat losses to the ambient air. The temperature in the tank is regulated by an electronic temperature controller and a variable transformer in conjunction with two band heaters covering the complete cylindrical outside surface. Before re-entering the tank, the condensate is heated to the saturation temperature of the solution by a separate heater. The pressure in the apparatus is monitored continuously and a pressure relief valve is installed for safety reasons. Boiling occurs at the outside of a cylindrical stainless steel test heater with a diameter of 10.67 mm, and a heated length of 99.1 mm. The test heater consists of an internally heated stainless steel sheathed rod and four stainless steel sheathed thermocouples with an outside diameter of 0.25 mm are embedded along the circumference of the heater close to the heating surface. Details of the test heater are given in Fig. 2. One thermocouple within the heated section was used as a safety trip, to cut off the power if the thermocouple temperature exceeded 170 °C. The test heater is manufactured by Drew Industrial Chemicals Company according to specifications by Heat Transfer Research Incorporated (HTRI).

A PC-based data acquisition system was used to measure temperatures, pressure and heat flux. The power supplied to the test heater could be calculated from the measured current and voltage drop. The average of five readings was used to determine the difference between wall and bulk temperature for each thermocouple. The temperature drop between the location of the wall thermocouples and the heat transfer surface was deducted from the measured temperature difference according to:

$$T_s - T_b = (T_{th} - T_b) - \left(\frac{s}{\lambda}\right)\dot{q} \tag{1}$$

In this equation, s is the distance between the thermocouple location and the heat transfer surface and λ is the thermal conductivity of the heater material. The value of s/λ was determined for each thermocouple by calibration of the test heater. The average temperature difference was the arithmetic average of the four thermocouple locations. The heat transfer coefficient α is calculated from:

$$\alpha = \frac{\dot{q}}{(T_s - T_b)_{av}} \tag{2}$$

For each heat flux, pictures of the heat transfer surface were taken using a micro-processor controlled camera with dedicated flash. Additionally, a standard VHF video camera was used to record the formation and

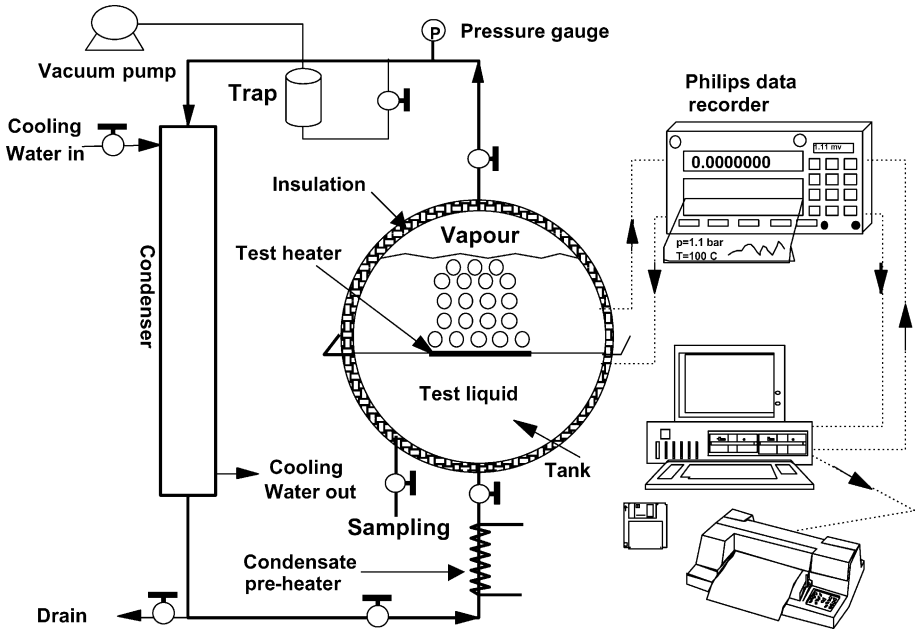

Fig. 1. Schematic diagram of pool boiling apparatus.

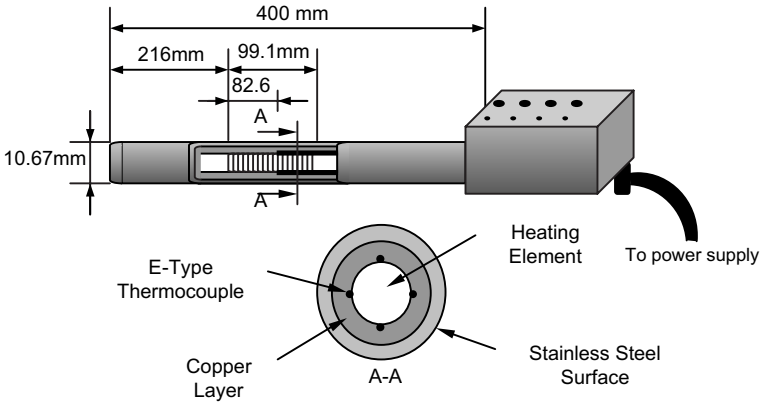

Fig. 2. Schematic drawing of test section.

growth of bubbles at the heat transfer surface. These recordings were then used to determine the bubble departure diameter.

2.1. Experimental procedure

Initially, test section and tank were cleaned and the system connected to a vacuum pump. Once the pressure of the system reached approximately 10 kPa, the test solution was introduced. Following this, the tank heater was switched on and the temperature of the system allowed to rise. Once the system was de-aerated it was left at the desired pressure and the corresponding saturation temperature for about five hours to obtain a homogenous condition throughout. Then, the power was supplied to the test heater and kept at a predetermined value. Data acquisition system, camera or video equipment were simultaneously switched-on to record temperatures, pressure, heat flux and visual information. All experimental runs were carried out with decreasing heat flux. Some runs were repeated later to check the reproducibility of the experiments, which proved to be excellent.

3. Test solutions and range of parameters

Heat transfer experiments were performed with aqueous solutions of the following salts: NaCl, Na_2SO_4 and KNO_3. The criteria for selecting the salts were based

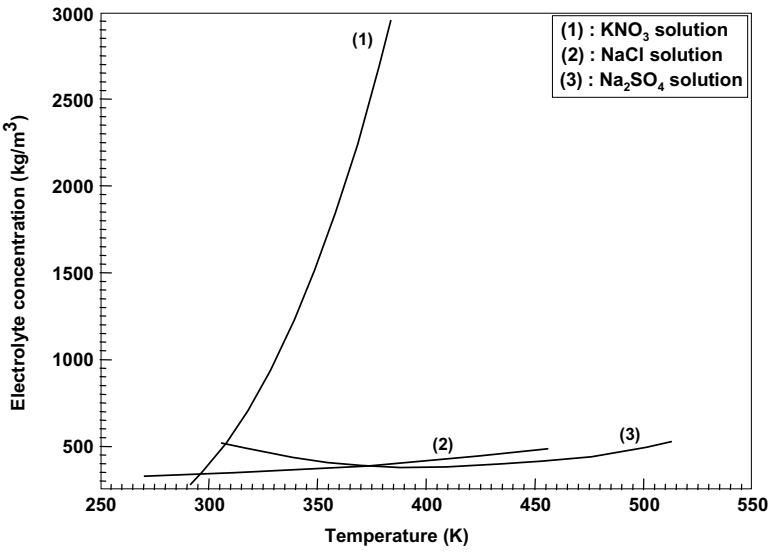

Fig. 3. Solubility of various electrolytes in water.

on the solubility of the salts, and the valence and size of the respective ions. The strength of the electrolyte solutions is generally defined by the ionic strength according to equation (3) [15]:

$$I = \frac{1}{2}\sum_j m_j Z_j^2 \tag{3}$$

This generalized parameter is essentially independent of the kind of electrolyte and depends only on the molar concentrations of the various ions in the solution and their respective charges.

The solubilities of the salts are given in Fig. 3 as a function of temperature. For the heat transfer surface temperatures used in this investigation, the saturation solubilities of Na_2SO_4 and NaCl are nearly independent of the temperature and the investigated concentrations are far away from the saturation point. The solubility of KNO_3 in water increases sharply with increasing temperature. Therefore, it is safely expected that no deposits form on the surface of the heating element in the range of concentrations which is used in this investigation. The range of operating conditions used in this investigation is given in Table 1.

The boiling temperatures of aqueous solutions of these salts are given in Fig. 4 as a function of salt concentration. The boiling point data can be fitted with excellent accuracy to the following general equation, over a wide range of salt concentrations:

$$T_b = a_0 + a_1 C^{a_2} \tag{4}$$

The fitted coefficients for the various salts are summarized in Table 2.

The physical properties of salt solutions and their boiling point data were taken from the International Critical Tables.

Table 1
Range of operating parameters

Heat flux	10–350 kW/m^2
Bulk temperature	100–110 °C
Salt concentration	
NaCl	1–80 kg/m^3
Na_2SO_4	1–150 kg/m^3
KNO_3	1–100 kg/m^3
Typical physical properties of solutions	
Density, ρ_l	900–1300 kg/m^3
Viscosity, μ_l	$(0.2–3.0)\times10^{-3}$ kg/m s
Specific heat capacity, c_p	3000–5000 J/kg K
Thermal conductivity, λ	0.5–0.8 W/mK
Surface tension, σ	70–80 N/m

Table 2
Coefficients for Eq. (4)

Solutions	a_0 (K)	a_1 (K m^3/kg)	a_2 (–)
Nacl	273.29	0.00589	1.223
Na_2SO_4	373.17	0.01293	0.906
KNO_3	373.17	0.0154	0.886

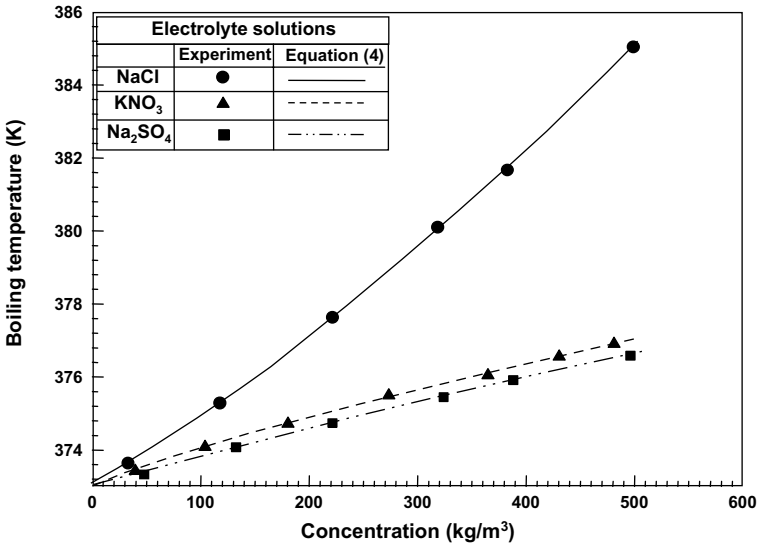

Fig. 4. Boiling temperature of electrolyte solutions as a function of concentration.

4. Results and discussion

Fig. 5 compares measured pool boiling heat transfer coefficients for electrolyte solutions over a wide range of ionic strength with values obtained for distilled water under identical operating conditions. The experimental data for distilled water are also compared with the prediction of the correlation suggested by Gorenflo [16] in which the relative influences of the main variables on the heat transfer coefficient are considered separately by F_q for the heat flux, F_p for the saturation pressure, and F_{WR} and F_{WM} for microstructure and material of the heating surface, respectively.

$$\alpha_w = \alpha_0 \cdot F_q \cdot F_p \cdot F_{WR} \cdot F_{WM} \tag{5}$$

with

$$F_q = \left(\frac{q}{q_0}\right)^n, \quad n = n(p_r) = 0.9 - 0.3p_r^{0.3} \tag{6}$$

$$F_p = 1.2p_r^{0.27} + 2.5p_r + \frac{p_r}{1-p_r} \tag{7}$$

$$F_{WR} = \left(\frac{R_a}{R_{a0}}\right)^{0.133} \tag{8}$$

and

$$F_{WM} = \left(\frac{\lambda\rho c}{\lambda_0\rho_0 c_0}\right)^{0.25} \tag{9}$$

The effect of surface roughness on the heat transfer coefficient is small and was neglected for the present investigation. For distilled water the reference heat transfer coefficient α_0 for a reference heat flux $q = 20$ kW/m^2 and a reference pressure $p_r = 0.1$ is 6 kW/m^2 K. As depicted in Fig. 5, the agreement between experimental data and predicted values is acceptable.

For low and moderate heat fluxes, the heat transfer coefficients of the electrolyte solutions are lower than those of distilled water. However, with increasing heat flux, this difference is reduced. A clear improvement in heat transfer was found at high heat fluxes. This phenomenon is related to bubble growth dynamics and bubble breakup in electrolyte solutions [17]. During pool boiling of distilled water at low heat fluxes, bubbles were uniform and the average bubble size was about 2 mm. At high heat fluxes larger bubbles were observed due to bubble interaction and bubble coalescence. Fig. 6 shows the appearance of the heat transfer surface during pool boiling of Na_2SO_4 solution for three different heat fluxes. At heat fluxes below 220 kW/m^2, because of the high interfacial tension, large hemispherical bubbles were observed and few nucleation sites are active on the heat transfer surface. Therefore, the heat transfer coefficients were lower than those of distilled water. When the heat flux was increased above 220 kW/m^2, bubble breakup became prevalent, the large bubbles disappeared and many small, rigid bubbles were formed. Formation of these small bubbles and their subsequent release into the surrounding liquid increases convection currents around the heater and consequently the heat transfer coefficient. Fig. 7 shows bubble diameter as a function of heat flux over a wide range of ionic strengths.

The presence of a small amount of electrolyte in water is sufficient to increase the bubble size in the low heat flux regime significantly. Any further increase in

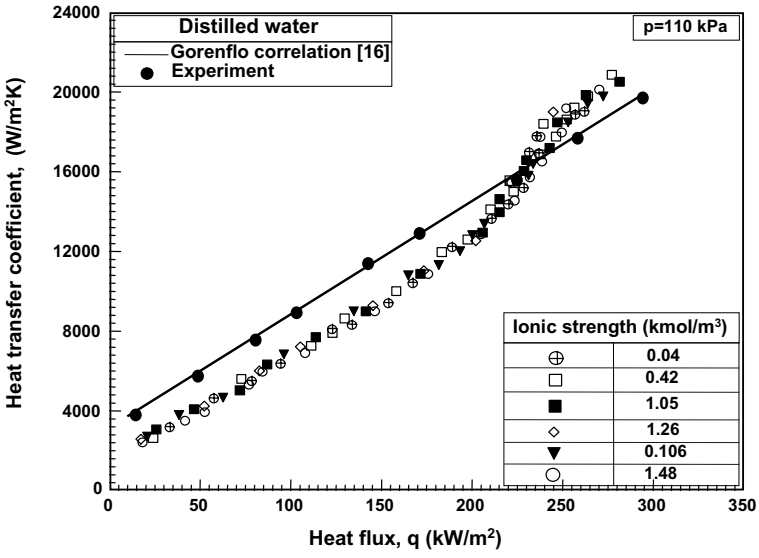

Fig. 5. Heat transfer coefficients for pool boiling of electrolyte solutions.

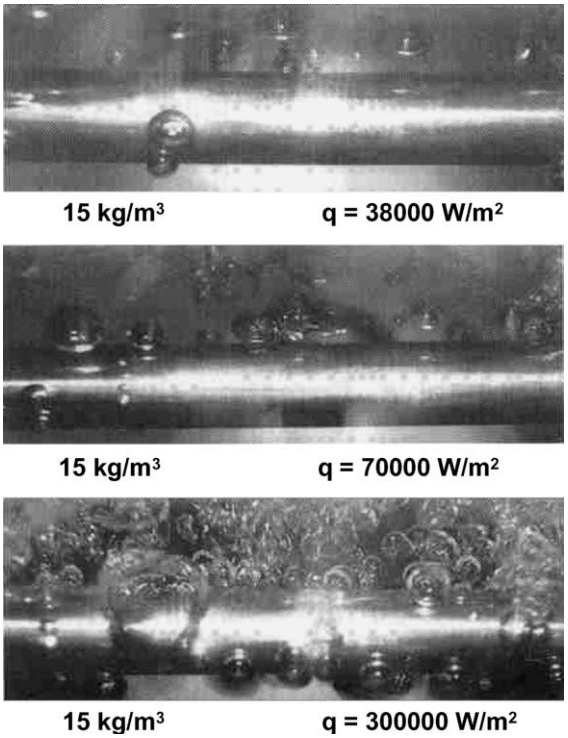

Fig. 6. The appearance of the heat transfer surface during boiling of Na_2SO_4 solution.

electrolyte concentration has only a minor effect. The measured bubble sizes have been compared with the prediction of several correlations, as discussed by Wenzel [18]. Unfortunately none of the available correlations is applicable to electrolyte solutions. The effect of heat flux on the mean bubble departure diameter found in the present investigation on electrolyte solutions could be correlated by equation (10)

$$\frac{1}{d_b} = 96.75 + \frac{0.01425q}{\ln q} \tag{10}$$

with an absolute mean average error of only 5%. In this equation, the heat flux is in W/m^2 and the bubble departure diameter in m.

It is well known that an increase in boiling heat flux is always accompanied by an increase in both number of active nucleation sites and frequency of bubble emission. Fig. 8 compares the number of active nucleation sites of electrolyte solutions with those for distilled water, as a function of heat flux. The number of active nucleation sites increases with increasing heat flux until the surface of the heating element is completely covered with bubbles. It is apparent that the number of active nucleation sites is significantly decreased due to the presence of the dissolved salts. According to equation (11) a higher surface superheat is necessary to activate a given nucleation site in the electrolyte solutions, because of the increased surface tension:

$$p^*(T_s) - p = \frac{2\sigma}{r_c} \tag{11}$$

For a given heat flux, therefore, the number of active nucleation sites is decreased below that for distilled water by the addition of salts. For water, the bubble frequency varied between 11 and 24 bubbles per second, with an average around 18 bubbles per second. In electrolyte

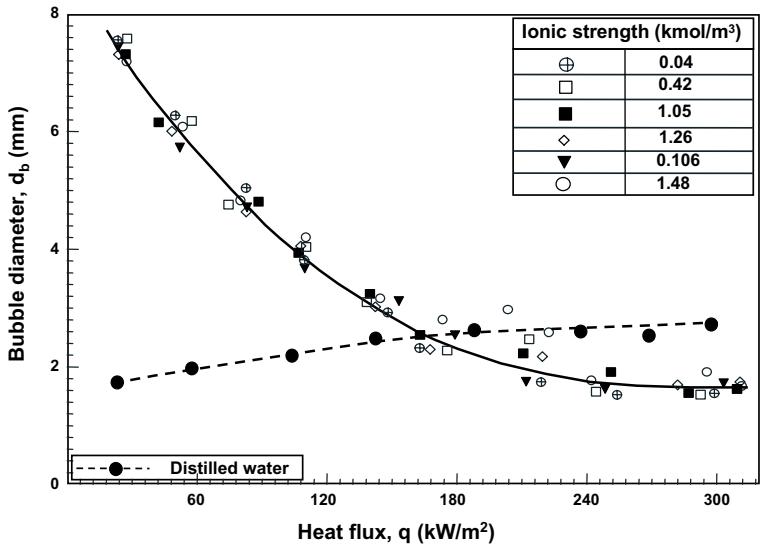

Fig. 7. Bubble departure diameter as a function of heat flux.

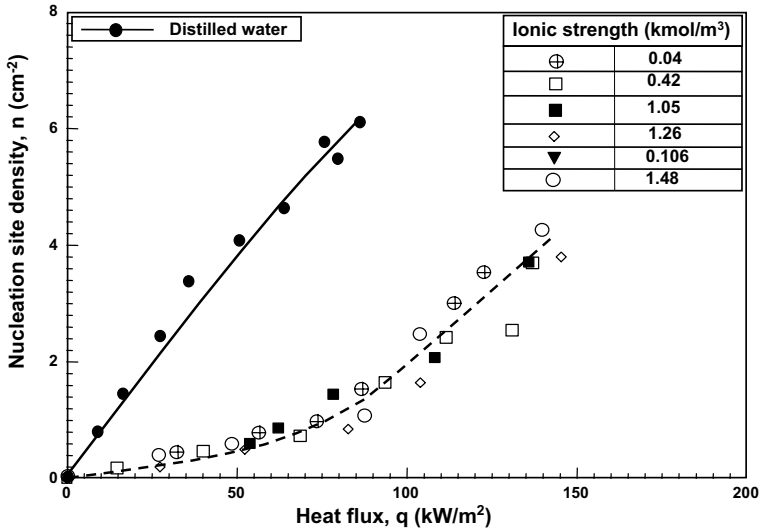

Fig. 8. Nucleation site density as a function of heat flux.

solutions, the bubble frequency was about 8 bubbles per second.

5. Modelling of heat transfer during pool boiling of electrolyte solutions

Fig. 9 serves to explain the heat transfer model for pool boiling of electrolyte solutions. Boiling heat transfer coefficients of pure fluids and mixtures are generally defined with the heat flux and the temperature difference between the measured heat transfer surface temperature and the bulk temperature:

$$\alpha = \frac{\dot{q}}{T_s - T_b} \tag{12}$$

However, the actual driving temperature difference $(T_s - T_i)$ is lower than $(T_s - T_b)$. This is due to the reduction in the interfacial mass fraction from x_w^b to x_w^i, due to the preferential evaporation of water, which causes the interfacial saturation temperature to rise by ΔT_i, from T_b to T_i.

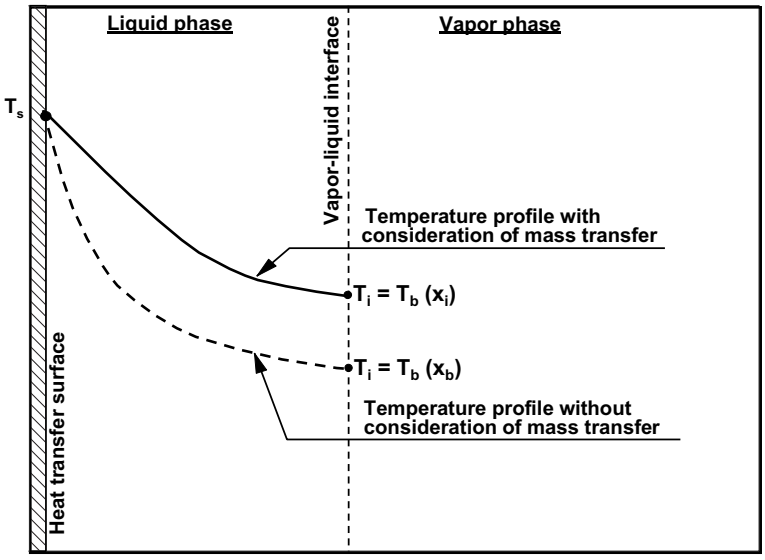

Fig. 9. Temperature profile during pool boiling of electrolyte solutions.

$$\Delta T_i = T_i - T_b \tag{13}$$

This rise in interfacial temperature is to a significant extent responsible for the apparent degradation of the pool boiling heat transfer coefficients of mixtures. The ideal heat transfer coefficient may, therefore, be defined as:

$$\alpha_i = \frac{\dot{q}}{T_s - T_i} \tag{14}$$

Combination of Eqs. (12)–(14) yields:

$$\frac{1}{\alpha} = \frac{1}{\alpha_i} + \frac{\Delta T_i}{\dot{q}} \tag{15}$$

where ΔT_i is a function of thermodynamic and transport variables. α_i may be considered as the heat transfer coefficient of an hypothetical fluid with the same physical properties as the solution, but without any kinetic mixture effects. Therefore, for the evaluation of pool boiling heat transfer coefficients of electrolytes solutions both terms ΔT_i and α_i, are important.

6. Calculation of temperature shift ΔT_i

The general procedure for the calculation of the temperature shift is first to calculate the interfacial composition from mass transfer principles and then to estimate the surface temperature from boiling point data.

When a vapor bubble is formed, water is vaporized on its surface and electrolyte solute is not. Therefore, a concentration gradient will be established causing water to diffuse towards and electrolyte solute to diffuse away from the interface, as indicated in Fig. 10. Over a discrete time interval, water will have evaporated from the surface and electrolyte solute will tend to diffuse away. This results in a total pressure gradient which causes a bulk motion of water and electrolyte solute towards the interface, in addition to the transfer by diffusion [19]. Hence the total mass flux of water towards the interface relative to stationary coordinates is equal to:

$$n_w = j_w + \rho_w U \tag{16}$$

The mass average velocity, U, can be expressed in terms of the mass concentration and the velocity of the species to a fixed coordinate as [20]:

$$U = \frac{\rho_w u_w + \rho_s u_s}{\rho_w + \rho_s} = \frac{n_w + n_s}{\rho} \tag{17}$$

Replacing Eq. (17) into Eq. (16) and using Fick's first law yields:

$$n_w = -\rho D \frac{\partial x_w}{\partial z} + x_w (n_w + n_s) \tag{18}$$

Under steady state conditions (i.e. n_w and n_s remain constant) the variables in Eq. (18) can be easily separated and integrated between bulk and interface. The result for water will be:

$$n_w = r_w \beta \rho \ln\left(\frac{r_w - x_w^i}{r_w - x_w^b}\right) \tag{19}$$

where β is the mass transfer coefficient and r_w is defined as

$$r_w = \frac{n_w}{n_w + n_s} \tag{20}$$

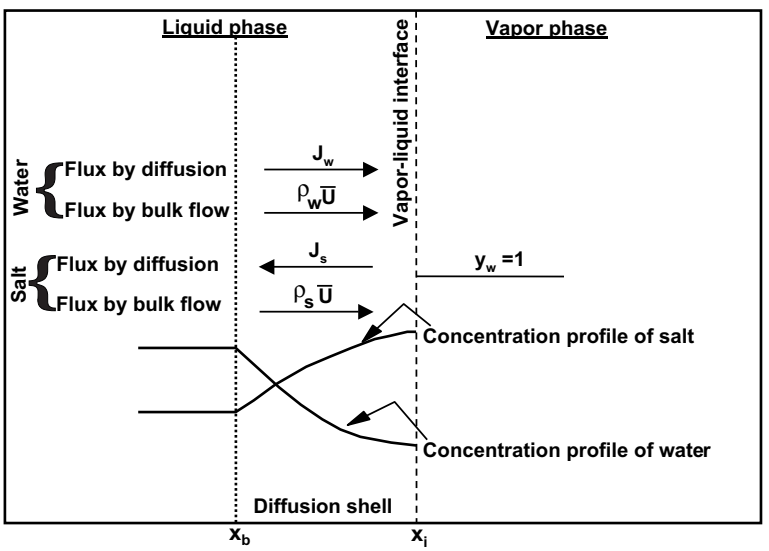

Fig. 10. Concentration profile and mass transfer rates through a mass diffusion shell surrounding the vapour bubbles.

Eq. (19) can be expressed as follows:

$$\frac{r_w - x_w^b}{r_w - x_w^i} = e^{-\theta} \tag{21}$$

$$\theta = \frac{n_w}{r_w \rho \beta} \tag{22}$$

Eq. (21) can also be derived from the Stefan-Maxwell equations. The value of n_w is approximated by Schlünder [21], assuming that during pool boiling all of the heat flow from the heat transfer surface passes into the bubbles in the form of latent heat:

$$\theta = \frac{B_0 \dot{q}}{r_w \rho \beta \Delta h_v} \tag{23}$$

The average diffusivity of water in electrolyte solutions and the resulting diffusion film thickness are 2×10^{-9} m^2/s and 10^{-5} m, respectively. Therefore, a constant mass transfer coefficient of 2×10^{-4} m/s has been used for the present work. B_0 is the ratio of the heat transfer surface to the mass transfer surface. It is assumed to be equal to unity by all investigators [18,22].

7. Interfacial composition of electrolyte

The counterpart of Eq. (16) for the electrolyte solute is:

$$n_s = j_s + \rho_s U \tag{24}$$

Since there is no net motion of electrolyte solute, the bulk rate of flow of solute towards the interface must exactly balance its transfer by back-diffusion from the interface. Thus Eq. (24) reduces to:

$$n_s = 0 \tag{25}$$

Replacing into Eq. (20) yields:

$$r_w = 1 \tag{26}$$

and Eq. (21) becomes:

$$\frac{1 - x_w^b}{1 - x_w^i} = e^{-\theta} \tag{27}$$

$$\frac{x_s^i}{x_s^b} = e^{\theta} \tag{28}$$

Hence the interfacial temperature can be obtained by substituting Eq. (28) into Eq. (4):

$$T_i = a_0 + a_1 C_b^{a_2} \exp(-a_2 \theta) \tag{29}$$

The ratio of the interfacial temperature, T_i, and the bulk temperature, T_b becomes:

$$\frac{T_i}{T_b} = \frac{a_0 + a_1 C_b^{a_2} \exp(-a_2 \theta)}{a_0 + a_1 C_b^{a_2}} \tag{30}$$

Eqs. (28) and (30) can be used to calculate the ratio of concentration and temperature at the interface to their values in the bulk of the solution. The results of these calculations for various solutions are summarized as a function of heat flux in Fig. 11. The concentration ratio increases strongly with heat flux while the temperature ratio is almost independent of the heat flux. The reason for this behavior can be found from the boiling point curves of electrolyte solutions in Fig. 4. These curves illustrate that doubling the concentration of electrolytes has only a small effect on the boiling point of the solutions in the range of electrolyte concentrations used in this investigation. Therefore, the second term in Eq. (15), has little effect on the deterioration of the heat transfer coefficient of the electrolyte solutions.

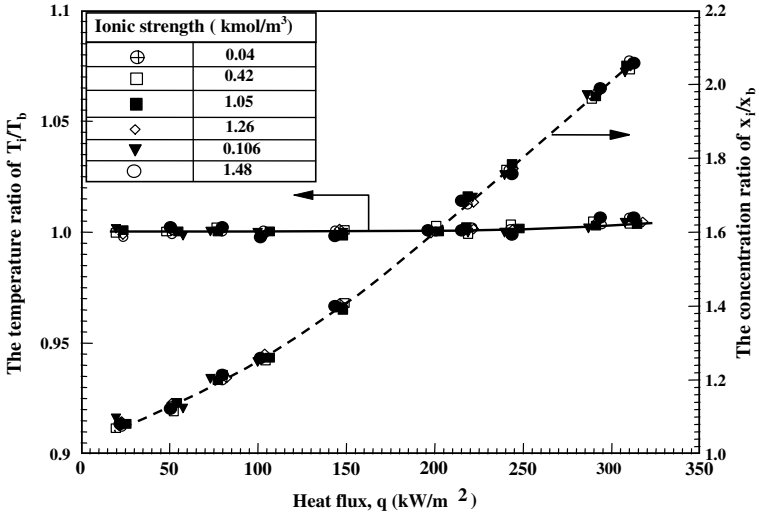

Fig. 11. The ratio of electrolyte concentrations and temperatures at interface and bulk as a function of heat flux.

In the present investigation, heat fluxes have been varied from 0 to350 kW/m^2. With a density of water $\rho = 1000$ kg/m^3 and a latent heat of evaporation of $\Delta h_v = 2257$ kJ/kg, Eq. (22) predicts values of θ in the following range:

$$0 \leqslant \theta \leqslant 0.72 \tag{31}$$

Applying these conditions to Eq. (28), it follows that

$$1 \leqslant \frac{x_s^i}{x_s^b} \leqslant 2.05 \tag{32}$$

Eq. (32) identifies the range of the ratio of the concentration of the electrolyte solute at the interface to its value in the bulk of the solution. This is also a crucial parameter for the study and modeling of scale formation under boiling conditions. Formation of deposits occurs when the saturation concentration of a dissolved salt is exceeded for the conditions at the heat transfer surface. From the above, an average ratio of interface to bulk concentration of about 1.5 may be expected. This value is in excellent agreement with the empirical value of 1.49, which has been obtained by Najibi et al. [23] from calcium sulfate scale formation experiments during subcooled flow boiling.

8. Calculation of α_i

The ideal heat transfer coefficient, α_{id}, is the boiling heat transfer coefficient the mixture would be expected to have without any resistance to mass transfer. For pool boiling of organic mixtures, it frequently defined as:

$$\frac{1}{\alpha_{id}} = \sum_{j=1}^{n} \frac{x_j}{\alpha_j} \tag{33}$$

where α_j represents the heat transfer coefficient of the pure component at the same heat flux as the mixture. For electrolyte solutions this reduces to:

$$\frac{1}{\alpha_{id}} = \frac{x_w}{\alpha_w} + \frac{1 - x_w}{\alpha_s} \tag{34}$$

For solutions with concentrations up to 10 kg/m^3 the bulk mass fraction of water is almost equal to unity ($x_w \approx 1$). With this assumption Eq. (34) reduces to:

$$\alpha_{id} \approx \alpha_w \tag{35}$$

Schlünder [21] assumed that the reduction of heat transfer coefficient of organic mixtures ($\alpha < \alpha_{id}$) is only caused by the use of a driving temperature difference based on the bulk temperature, T_b, rather than on the interface temperature T_i. This assumption would lead to the statement:

$$\alpha_i = \alpha_{id} = \alpha_w \tag{36}$$

if conditions are such that the difference between wall temperature and local saturation temperature is the same. Wadekar et al. [24] used Eq. (36) for the prediction of mixture effect in boiling of salt solutions with concentration up to 70 kg/m^3. The present experimental observations for boiling of electrolyte solutions strongly indicate, however, that α_i is not the same as α_w for distilled water. α_i can be easily estimated from the experimental data in conjunction with equations (4), (15) and (29). The results of these calculations for α_i are compared with those values for distilled water in Fig. 12. The

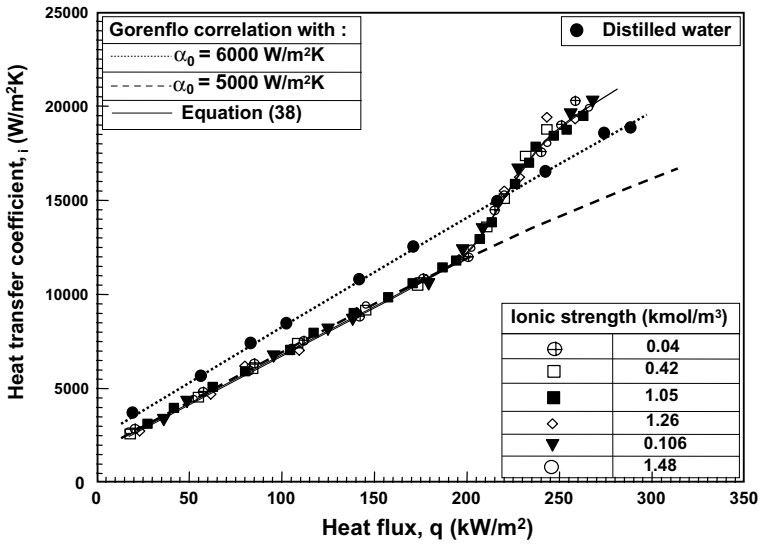

Fig. 12. Variation of measured and predicted ideal heat transfer coefficient with heat flux.

computed trend agrees with that for the measured heat transfer coefficient for electrolyte solutions in Fig. 5. The results show that at heat fluxes lower than 220 kW/m^2, the ideal heat transfer coefficients α_i are lower than those for distilled water while at higher heat flux the ideal heat transfer coefficient is higher, as a result of the dispersion of the large bubbles.

The general approach for the calculation of α_i is to use a pure fluid boiling correlation with physical properties of the mixture. The reference heat transfer coefficient, α_0, for a reference heat flux $q = 20$ kW/m^2 and a reference pressure $p_r = 0.1$ in the Gorenflo correlation may be determined using the correlation suggested by Stephan and Preusser [25]. Unfortunately this model is very sensitive to the bubble departure diameter and independent of nucleation site density. Therefore, a reference value α_0 of 5 kW/m^2 K is determined from the experimental data. The result of this procedure is also shown Fig. 12. For heat fluxes less than 220 kW/m^2, the predicted values are now in excellent agreement with the experimental results, while for higher heat fluxes the variation between the predictions and experimental data is quite considerable. These results clearly indicate the shift of heat transfer characteristics when the transition into the bubble breakup regime occurs. Such a behavior can be well presented by a "sigmoid" function:

$$F_2 = \frac{b_0}{1 + e^{-b_1(q-220)}} \tag{37}$$

The constants b_0 and b_1 are known as "gain" and "steepness" parameters and vary between 0 and 1. For heat fluxes less than 220 kW/m^2, the response of Eq. (37) is zero but for higher heat fluxes the value of this function smoothly increases to the value of b_0. The numerically determined values of gain and steepness parameters from the experimental data are 0.42 and 0.15 respectively. Replacing these parameters into Eq. (37) yields after some mathematical manipulations:

$$\alpha_i = \alpha_{Go} + \frac{0.42}{1 + e^{-0.15(q-220)}}\alpha_{Go} \tag{38}$$

where α_{Go} is the predicted value of the Gorenflo correlation with a reference heat transfer coefficient of 5 kW/m^2 K. The prediction of Eq. (38) is also shown in Fig. 12. The calculated trend is in excellent accordance with the values obtained from the experimental data. The absolute mean average error of 2% confirms that the correlation is very suitable for the prediction of the ideal heat transfer coefficient, α_i, of the investigated electrolyte solutions.

9. Comparison with measured heat transfer coefficients

Writing Eq. (4) for interface and bulk concentrations of the solution and then subtracting them from each other yields:

$$\Delta T_i = T_i - T_b = a_1 (C_s^b)^{a_2} \left[\left(\frac{C_s^i}{C_s^b} \right)^{a_2} - 1 \right] \tag{39}$$

Substituting Eq. (28) into Eq. (39) yields:

$$\Delta T_i = a_1 [C_s^b]^{a_2} [\exp(a_2 \theta) - 1] \tag{40}$$

Therefore, the heat transfer coefficient for electrolyte solutions can be obtained by substituting of Eq. (40) and (38) into Eq. (15).

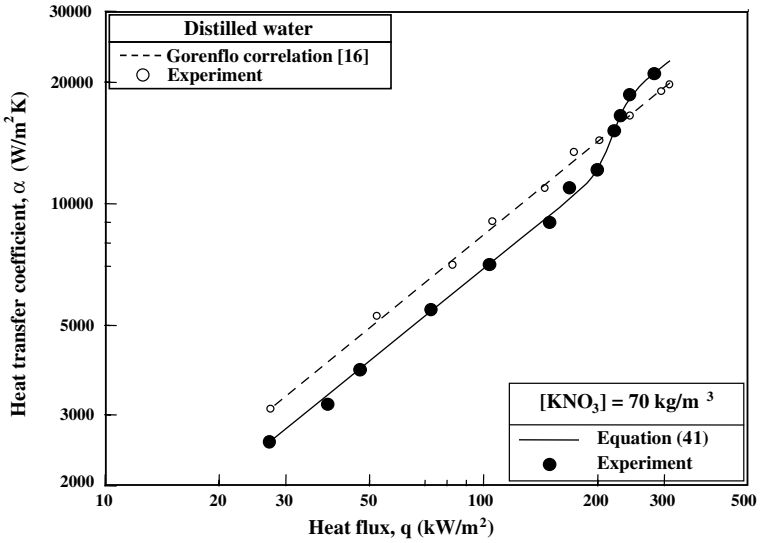

Fig. 13. Measured and predicted heat transfer coefficient for typical KNO_3 solution.

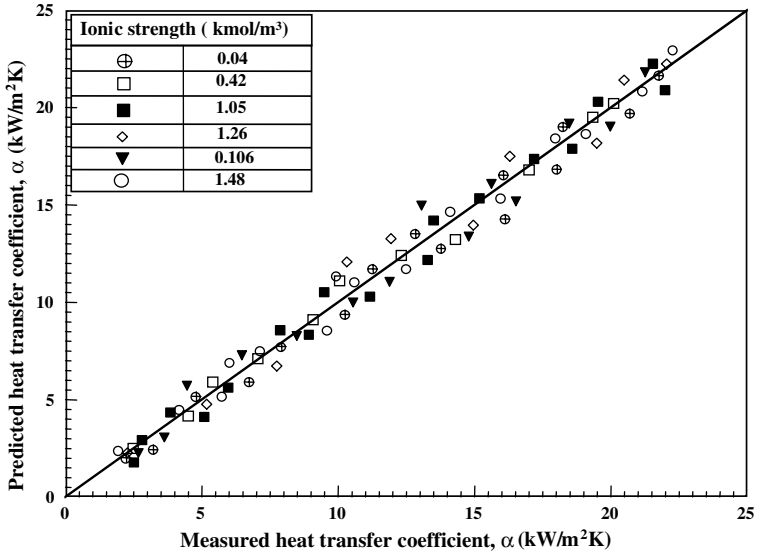

Fig. 14. Comparison of measured and predicted pool boiling heat transfer coefficients for electrolyte solutions.

$$\frac{1}{\alpha} = \frac{1+\exp(33-0.15q)}{\alpha_{Go}(1.42+\exp(33-0.15q))} + \frac{a_1(C_s^b)^{a_2}}{\dot{q}} \times [\exp(a_2\theta)-1] \quad (41)$$

Hence Eq. (41) can be used to predict the heat transfer coefficients for electrolyte solutions. The predictions of the presented model as well as of the Gorenflo [16] correlation are shown in Fig. 13 for an electrolyte solution with a concentration of 70 kg/m^3 KNO_3. The calculated values are in excellent qualitative and quantitative agreement with the experimental data. The applicability of this model for electrolytes with positive solubility is further demonstrated in Fig. 14 where all the experimental data over a wide range of concentrations are compared with values predicted from Eq. (41). The absolute mean average error between the predictions and the experimental heat transfer data is less than 8%, which shows the applicability of the model.

10. Conclusions

The presence of small amount of salts with positive solubility has a considerable effect on nucleate boiling heat transfer of water. At low heat fluxes, the bubble departure diameter increases and the heat transfer coefficient decreases. At high heat fluxes a large number of small bubbles is found on the heat transfer surface, and the heat transfer coefficient improves. Assuming that the decrease of heat transfer coefficient in pool boiling of electrolyte solution is the result of a mass transfer resistance in the liquid phase, a model was proposed which permits the determination of pool boiling heat transfer coefficients of electrolyte solutions with good accuracy.

References

[1] J.R. Welty, R.E. Wilson, C.E. Wicks, Fundamentals of Momentum Heat and Mass Transfer, second ed., John Wiley & Sons, 1984, pp. 551–560.
[2] W.R. Van Wijk, A.S. Vos, J.D. Van Stralen, Heat transfer to boiling binary liquid mixtures, Chem. Eng. Sci. 5 (1956) 68–80.
[3] C.V. Sternling, L.J. Tichacek, Heat transfer coefficients for boiling mixtures, Chem. Eng. Sci. 16 (1961) 297–337.
[4] J.R. Thome, Bubble growth and nucleate pool boiling in liquid nitrogen, argon and their mixtures, D.Phil. thesis, Oxford University, UK, 1978.
[5] J.R. Thome, Latent and sensible heat transfer rates in boiling of binary mixtures, J. Heat Transfer 104 (1982) 474–478.
[6] D.S. Cryder, E.R. Gilliland, Heat transmission from metal surfaces to boiling liquids, Ind. Eng. Chem. 24 (1932) 1382–1387.
[7] D.S. Cryder, A.C. Finalboro, Heat transmission from metal surfaces to boiling liquids: effect of temperature of the liquid on the liquid film coefficients, AIChE Trans. 33 (1937) 347–361.
[8] J.W. Knowles, Heat transfer with surface boiling, Can. J. Res. 26 (1948) 268–278.
[9] V.I. Tolubinsky, J.N. Ostrovsky, On the mechanism of boiling heat transfer, Int. J. Heat Mass Transfer 9 (1966) 1463–1470.
[10] D. Steinbrecht, Beitrag zur Untersuchung der Dampfblasenbildung bei Mehrstoffgemischen, Wiss. Z. Tech. Hochsch. Magdeburg 12 (1968) 505–513.
[11] W. Fritz, Berechnung des Maximalvolumens von Dampfblasen, Phs. Z. 36 (1935) 379–384.
[12] W.C. Ceumern-Lindenstjerna, Bubble departure diameter and release frequencies during nucleate pool boiling of water and aqueous sodium chloride solutions,

in: E. Hahne, U. Grigull (Eds.), Heat Transfer Boiling, Hemisphere, New York, 1997, pp. 53–75.
[13] K. Feldkamp, Der Wärmeübergang beim Sieden von wässrigen lösungen, in: Proc. 4th Int. Heat Transfer Conf. 1970, paper B7.2.
[14] M. Jamialahmadi, H. Müller-Steinhagen, Pool boiling heat transfer to electrolyte solutions, Chem. Eng. Process 28 (1990) 79–88.
[15] D.A. Skoog, D.M. West, Fundamentals of analytical chemistry, fourth ed., CBS College publishing Co., 1982.
[16] D. Gorenflo, State of the art in pool boiling heat transfer of new refrigerants, Int. J. Refrig. 24 (2001) 6–14.
[17] S.H. Najibi, H. Müller-Steinhagen, M. Jamialahmadi, Boiling and non-boiling heat transfer to electrolyte solutions, Heat Transfer Eng. 17 (1996) 46–63.
[18] U. Wenzel, Saturated pool boiling and subcooled flow boiling of mixtures, Ph.D. thesis, University of Auckland, New Zealand, 1992.
[19] J.M. Coulson, J.F. Richardson, in: Chemical Engineering, vol. 1, Pergamon Press, 1977, pp. 268–276.
[20] A.L. Hines, R.N. Maddox, Mass transfer fundamentals and applications, Prentice-Hall, Englewood, NJ, 1985.
[21] E.U. Schlünder, Heat transfer in nucleate boiling of mixtures, Int. Chem. Eng. 23 (1983) 589–599.
[22] V.V. Wadekar, Convective heat transfer of binary mixtures in annular two-phase flow, in: Proceedings of the 10th Int. Heat Transfer Conf., Brighton, vol. 7, 1994, pp. 557–562.
[23] H. Najibi, M. Jamialahmadi, H. Müller-Steinhagen, Calcium sulphate scale formation during subcooled boiling, Chem. Eng. Sci. 52 (1997) 1265–1284.
[24] V.V. Wadekar, P.D. Hills, J. Mattes, Mixture effect in boiling of salt solutions, in: Heat Transfer—Baltimore, AIChE Symposium Series, vol. 93, 1997, pp. 233–238.
[25] K. Stephan, P. Preusser, Wärmübergang und maximale Wämestromdichte beim Behältersieden binärer und ternärer Flüssigkeitsgemische, Chem. Ing. Tech. MS 649/79 (1979).